Optimization of the recollision step in high-order harmonic generation

Michael Klaiber, Markus C. Kohler, Karen Z. Hatsagortsyan, and Christoph H. Keitel
Max-Planck-Institut für Kernphysik, Saupfercheckweg 1, 69117 Heidelberg, Germany
(Received 16 February 2012; published 25 June 2012)

The recombination step of high-order harmonic generation is investigated with the aim of optimizing the high-energy photon emission yield in this process. The dependence of the recombination probability of a recolliding electron on the parameters of the atomic potential, such as its width and depth and the parameters of the electron wave packet such as its impact parameter, width, and angular momentum, are analyzed. Empirical laws for these parameters are found that ensure optimal recombination and in this way optimal emission of high-energy photons.

DOI: 10.1103/PhysRevA.85.063829 PACS number(s): 42.65.Ky, 34.50.Rk

I. INTRODUCTION

High-order harmonic generation (HHG) [1] has been developed into a reliable source of coherent extreme ultraviolet radiation and is expected to be extended into the soft x-ray region up to kilo-electronvolt photon energies [2–6]. A further increase of the photon energy can, in principle, be achieved by increasing the laser intensity. Although it is well known that the applicable laser intensities are limited by the relativistic electron drift, which prevents recollision, and by a large free electron dispersion, which causes a significant phase-mismatch [7,8], there are ways to overcome these problems [9,10]. Nevertheless, there are more fundamental restrictions which hinder realization of HHG at higher photon energies [9]: even for a suppressed relativistic drift, the HHG photon yield decreases dramatically with rising photon energy due to the reduced recombination cross section and the increased emission bandwidth at a fixed ionization window [9]. In this context, it is particularly important to find conditions optimizing the recombination step.

HHG is intuitively explained in the three-step model [11,12]. In the first step, the active electron is tunnel-ionized from the atomic system; in the second step, it is propagated in the continuum by the laser field; finally, in the third step, it is driven back, recolliding with the atomic system and emitting its gained energy as a high-frequency photon. Each step of HHG has a well-defined probability and thus the overall probability for emission of a highly energetic photon results from the probabilities of the single steps [13,14]. The probability for tunnel ionization is well described by the quasiclassical Perelomov, Popov, Terent'ev (PPT) ionization rates [15,16]. The continuum dynamics is quasiclassical, resulting in the spreading of the electron wave packet, (see, e.g., Ref. [17]). The recollision probability of the laser-driven electron, in general, depends on the shape of the atomic potential (in particular, on its width and depth parameters), as well as on the size of the electron wave packet, its momentum distribution, and the impact parameter. Driving the HHG process effectively demands optimization of all three steps.

Enhanced recombination probabilities during the third step have been discussed in connection with multielectron effects recently. The calculations reported in Ref. [18] show a general enhancement of the recombination probability with the number of bound electrons due to polarization recombination [19,20]. The experimental studies of Ref. [21] concentrate on the giant resonance in xenon known from its ionization dynamics for a long time. Their calculation shows that the enhancement in HHG spectra can be explained via the excitation of a tightly bound electron to the valence shell by the recolliding electron simultaneous with the recombination of the continuum electron to this deeper-lying shell. However, the contribution of the atomic shell polarization in recombination decreases sharply when the recombining electron energy exceeds the ionization potential of the K shell, reducing the recombination cross section to that of an electron on the atomic nuclei [19].

In this paper we investigate the recombination step of HHG at high energies of the recolliding electron, such that the atomic shell polarization is negligible, with the perspective of gaining more insight into how the production of high-frequency photons via HHG can be upgraded in the case of a one-electron atomic or ionic system. With the goal of finding optimal conditions for the recollision step, we investigate the recollision for different atomic potentials and find the potential parameters that are best suited for effective recombination. In particular, in the case of a spatially broad recolliding electron wave packet and large electron energy exceeding the absolute value of the bound state energy, it is found that recollision yields are favorable when the characteristic radius of the atomic potential is less than the de Broglie electron wavelength. Further, we investigate the impact of the characteristics of the recolliding electron wave packet on the recombination probability. In the case of a broad recolliding electron wave packet in momentum space, it is found that the recombination is optimal when the momentum width of this wave packet is of the order of its mean momentum. Thus even for a very broad recolliding wave packet in momentum space at high mean energies, as is usual at very strong laser fields, efficient recombination yields are feasible. The considerations in the paper are based on the strong field approximation (SFA) [22–24].

The structure of the paper is as follows. In Sec. II we investigate how the process is described most accurately within SFA, comparing the transition matrix element from the initial exact continuum state with that using an initial plane-wave state. Section III is devoted to the optimization of parameters of the atomic potential and Sec. IV to that of the electron wave packet. In Sec. V we present applications of our findings. The conclusion is given in Sec. VI.

II. THE CHOICE OF GAUGE IN THE RECOLLISION MATRIX ELEMENT

The Hamiltonian of the considered system can be written as follows:

$$H = H^V + V(\mathbf{r}) + H_i, \tag{1}$$

where H^V is the Volkov-Hamiltonian of the electron in the laser field, $V(\mathbf{r})$ the atomic potential, and H_i the Hamiltonian of the electron interaction with the harmonic field. The latter is described in second quantization and can be treated as a perturbation. Our discussion is based on the description of the HHG process within the SFA. The differential rate of the nth harmonic emission during the recombination of the laser-driven electron reads [25]

$$\frac{dw_n}{d\Omega} = \frac{(n\omega)^2}{(2\pi)^2 c^3}\left|\int_0^T \frac{dt}{T}\langle\phi_0(t),1_H|H_i|\psi^{\mathrm{SFA}}(t),0_H\rangle\right|^2, \tag{2}$$

where $|\phi_0,1_H\rangle \equiv |\phi_0\rangle|1_H\rangle$ and $|\psi^{\mathrm{SFA}},0_H\rangle \equiv |\psi^{\mathrm{SFA}}\rangle|1_H\rangle$, with the bound state $|\phi_0\rangle$ of the electron and the harmonic field state with n photons $|n_H\rangle$. c is the speed of light, ω the laser angular frequency, and T the laser period. Atomic units are used throughout the paper. The electron continuum state in the SFA reads [26]

$$|\psi^{\mathrm{SFA}}(t)\rangle = \int_{-\infty}^{t} d\tilde{t}\,U^V(t,\tilde{t})V(\mathbf{r})|\phi_0(\tilde{t})\rangle, \tag{3}$$

where U^V represents the Volkov time-evolution operator. The differential emission rate can then be written as

$$\frac{dw_n}{d\Omega} = \frac{(n\omega)^2}{(2\pi)^2 c^3}\left|\int_0^T \frac{dt}{T}\int_{-\infty}^{t} d\tilde{t}\langle\phi_0(t),1_H|H_i U^V(t,\tilde{t}) \times V(\mathbf{r})|\phi_0(\tilde{t}),0_H\rangle\right|^2. \tag{4}$$

From this expression the three steps consisting of ionization, free propagation, and recombination can be identified [14]. In the SFA, the state of the electron is approximated by a plane wave and the probability of the electron recombination with an emission of a harmonic photon is proportional to the squared matrix element of H_i:

$$P = |\langle\mathbf{p},0_H|H_i|\phi_0,1_H\rangle|^2, \tag{5}$$

with the momentum $\mathbf{p}$ at the moment of recollision.

The form of H_i depends on the adopted gauge. Three different forms of the interaction Hamiltonian are well known: the length $H_i^L = \mathbf{r}\cdot\mathbf{E}_H$, the velocity $H_i^V = \mathbf{p}\cdot\mathbf{A}_H$, and the acceleration form $H_i^A = -\nabla V\cdot\boldsymbol{\alpha}_H$ with the harmonics electric field $\mathbf{E}_H = -\dot{\mathbf{A}}_H = -\ddot{\boldsymbol{\alpha}}_H$ in second quantization. In the case that the exact continuum state of the electron is employed in Eq. (5), taking into account the atomic potential explicitly, the recombination probability is gauge independent. However, when the state of the recolliding electron is approximated by a plane wave $|\mathbf{p}\rangle$ as in the standard SFA, these three forms are not equivalent and the question arises as to which form is best suited for the description of the recollision process. To answer this question, we calculate the recombination probability $P = |\langle\mathbf{p},0_H|H_i|\phi_0,1_H\rangle|^2$ for the transition from the plane-wave continuum state $|\mathbf{p}\rangle$ into the ground state $|\phi_0\rangle$ of the atomic potential using the interaction Hamiltonian H_i in all three forms and compare them with the case when the initial state is an exact continuum state of the atomic potential with an asymptotic momentum $\mathbf{p}$ (see Appendix). Note that in the last case the result is independent of the gauge. Three different atomic potentials are considered: a Coulomb potential

$$V^C(\mathbf{r}) = -\kappa/r, \tag{6}$$

a zero-range (ZR) potential

$$V^Z(\mathbf{r}) = -\frac{2\pi}{\kappa}\delta(\mathbf{r})\partial_r r, \tag{7}$$

and a radial symmetric box potential

$$V^B(\mathbf{r}) = -V_0\Theta(R-r), \tag{8}$$

with the typical momentum of the bound electron $\kappa = \sqrt{2I_p}$, the ionization potential I_p, and the Heaviside step function $\Theta(x)$. While the Coulomb and the ZR potentials depend only on a single parameter κ, the box potential is determined by two parameters: the box size R and the depth V_0. The box size R is a function of V_0 and κ:

$$R = \frac{\pi - \tan^{-1}(\sqrt{2V_0/\kappa^2 - 1})}{\sqrt{2V_0 - \kappa^2}}. \tag{9}$$

In Fig. 1 the recombination probability versus the momentum of the recolliding electron is displayed for the various gauges and potentials at a fixed κ. For the ZR potential, the transition matrix element is independent of the choice of the interaction Hamiltonian (because the continuum is not affected by the ZR potential) and coincides with the exact solution

$$P = \frac{2p^2\kappa}{\pi^2(p^2+\kappa^2)^3}. \tag{10}$$

Accordingly, a single line is plotted for the ZR potential in Fig. 1(a). However, for the Coulomb potential and the box potential, the exact results differ from the SFA results in the different gauges. The SFA results in acceleration form have the best agreement with the one obtained with exact continuum states for $p > \kappa$, while those in the velocity and length gauges largely deviate in the same parameter regime. For the length gauge, the deviation is more than an order of magnitude. This is in accordance with the numerical analysis given in Ref. [27]. For recolliding electron momenta $p \leqslant \kappa$, none of the three approximations can be favored and a deeper analysis via comparison with numerical calculations of the HHG process is needed [28]. We consider optimization of HHG for plateau harmonics, i.e., in the regime $p > \kappa$. Accordingly, a conclusion is drawn to employ the acceleration form of the recollision matrix element.

III. PARAMETERS OF THE ATOMIC POTENTIAL FOR EFFECTIVE RECOMBINATION

In this section, we investigate the influence of the atomic potential shape on the effectiveness of recollision. We compare the recombination probabilities for the three potentials at hand at a fixed binding energy I_p. In Fig. 2, the absolute squares of the recombination matrix elements P versus the momentum of the recolliding electron are displayed for the ZR, the Coulomb, and the box potential. In the latter case three different sizes

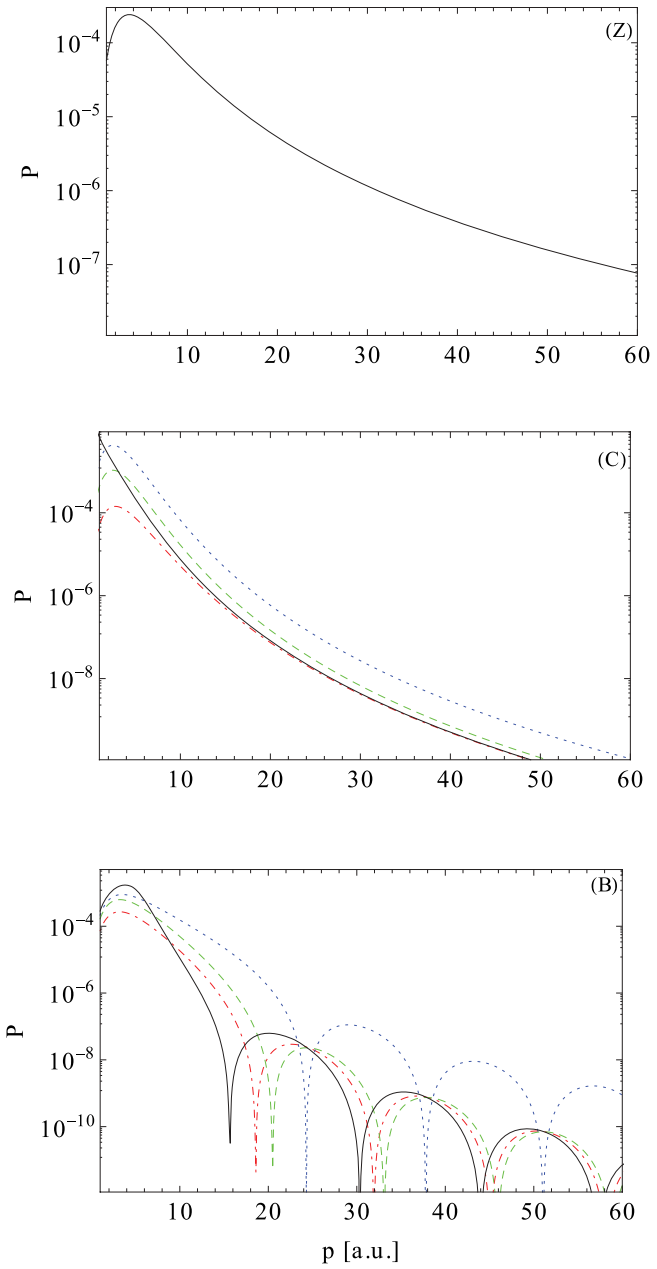

FIG. 1. (Color online) Recombination probability into a bound state with $\kappa = 5$ a.u. versus the electron recollision momentum for the (Z) zero-range, (C) Coulomb, and (B) box potential with $R = 0.25$ a.u., using different approximations: an exact continuum state for the recombining electron (solid black), and a plane-wave state for the recombining electron with the interaction Hamiltonian H_i in the length form (blue, dotted), velocity form (green, dashed), acceleration form (red, dashed-dotted). The curves corresponding to the exact continuum states are independent of the employed operator.

of the potential box are considered corresponding to the three parameter regimes: $R < 1/\kappa$, $R = 1/\kappa$, and $R > 1/\kappa$. The first can be seen as a model for a short-range potential, whereas the second has a size of the typical length of the Coulomb potential, and the third is a broad potential.

The following features can be recognized in Fig. 2. First, the Coulomb and ZR potentials can be modeled by the box potential, as long as the box size corresponds to the respective

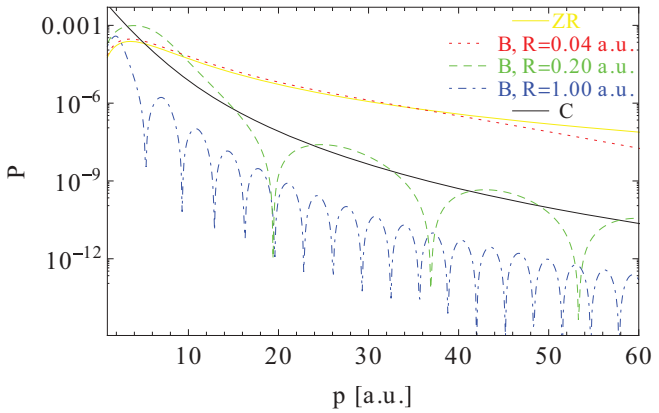

FIG. 2. (Color online) Recombination probability from the exact continuum states of the respective potential into a bound state with $\kappa = 5$ a.u. versus the electron recollision momentum for the Coulomb (black, solid), zero-range (yellow, gray solid), and box potentials, with a radius $R = 0.04$ a.u. (red, dashed), $R = 0.2$ a.u. (green, long-dashed), and $R = 1$ a.u. (blue, dot-dashed).

typical length. Then the envelope of the recombination probability for the box potential reproduces the one in the Coulomb and ZR potentials; only resonance effects due to the box form alter the probability curves. This also indicates that for the analysis of the recombination effectiveness more sophisticated potential forms are not required. Second, for $p > \kappa$ (here, $\kappa = 5$ a.u.) the recombination probability decreases with increasing p in all cases, and a narrow potential should be preferred in this parameter regime. This is because the matrix element P is proportional to the square of the Fourier component of the potential $|V_p|^2$ [38], which is constant in the case of the short-range potential (then $P \sim 1/p^4$, see the estimation in Ref. [32] and Eq. (10)) and $V_p \sim 1/p^2$ in the case of Coulomb potential ($P \sim 1/p^8$, see [32]). Third, in the area $p \approx \kappa$ all probabilities have a similar order of magnitude and the potential shape plays only a secondary role.

Using the box potential as a simple two-parameter model of any potential, we are now able to choose optimal conditions to enhance the recombination probability for a given momentum of the recolliding electron, i.e., at a fixed energy of the emitted harmonic photon. In the high-energy regime $p \gg \kappa$, the short-range potential is favored, as the estimation above and Fig. 2 show. The box potential can be regarded as short range when $R \ll 1/\kappa$ and additionally,

$$R \lesssim 1/p, \tag{11}$$

i.e., for a given momentum p of recolliding electron, the potential size should be chosen as $R \sim 1/p$ or smaller to have the largest probability; even smaller sizes do not improve recombination anymore. (The dashed line in Fig. 2, corresponding to the case of the box potential with $R = 0.04$ a.u., coincides with the case of ZR potential up to $p \sim 1/R$ and decreases at further increase of momentum.)

However, generally the $p \lesssim \kappa$ region is the most favorable for the recombination. Therefore, the dependence on the potential box size in this region is investigated next. In Fig. 3 the dependence of the recombination probability on the box size R and the bound-state parameter κ is shown. As one

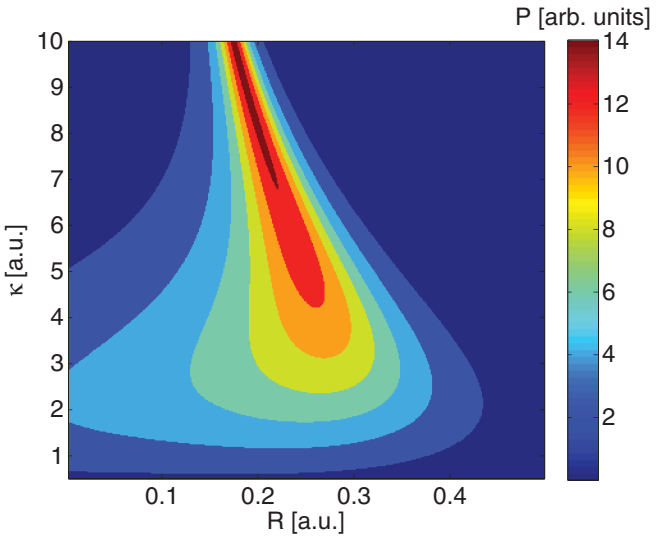

FIG. 3. (Color online) Recombination probability from the exact continuum states into the bound state versus the bound-state parameter $\kappa = \sqrt{2I_p}$ and the box size R for a fixed momentum $p = 5$ a.u. of the recolliding electron.

can see from Fig. 3, in the region $\kappa > p$ the recombination probability is sharply peaked at $R \sim 1/p$. In the $\kappa < p$ region, the optimal radius is in the domain around $R \sim 1/p$ but the dependence on the radius is rather smooth. The explanation for the "$pR \sim 1$" rule can be given via a partial wave analysis. The incoming plane wave consists of a superposition of spherical harmonics [29]:

$$\begin{aligned}\langle \mathbf{r}|\mathbf{p}\rangle &= \exp[i\mathbf{p}\cdot\mathbf{r}]/(2\pi)^{3/2} \\ &= \sum_{l=0}^{\infty} i^l(2l+1)j_l(pr)P_l(\cos[\theta])/(2\pi)^{3/2}, \quad (12)\end{aligned}$$

with the angular momentum quantum number l. Inserting this expansion into the matrix element for recollision into a $1s$ Coulomb state leads to

$$\begin{aligned}\langle \phi_0|\nabla V|\mathbf{p}\rangle &= \sum_{l=0}^{\infty} \frac{i\sqrt{2}\kappa^{5/2}\mathbf{p}[1-(\kappa/p)\arctan(p/\kappa)]}{\pi p^2}\delta_{l,1} \\ &= \frac{i\sqrt{2}\kappa^{5/2}\mathbf{p}[1-(\kappa/p)\arctan(p/\kappa)]}{\pi p^2}, \quad (13)\end{aligned}$$

which indicates that only the partial wave with an angular momentum $l = 1$ contributes to the transition, a property which is well known from the photoionization theory [30]. In the case for $l = 1$, the spherical Bessel function with an argument pr has a characteristic size of the order of $1/p$. Consequently, the overlap with the atomic system is the largest when the characteristic size of the impinging electron wave is comparable with the size of the atomic potential $R \approx 1/p$, which justifies the numerical analysis above.

Thus, for a recolliding electron with a fixed energy, the HHG is most effective when the typical parameter κ of the potential is of the order of the electron momentum and, further, when the potential radius $R \sim 1/p$. For the Coulomb potential in the $p \sim \kappa$ regime, the "$pR = 1$" rule is fulfilled automatically, indicating that hydrogenlike atoms are already the optimal choice for the atomic system in the HHG process in this parameter regime. In the high-energy regime $p \gg \kappa$, the short-range potential ($R \lesssim 1/p$) is most favorable for HHG.

IV. PARAMETERS OF THE RECOLLIDING ELECTRON WAVE PACKET FOR EFFECTIVE RECOMBINATION

In the previous section, we considered the case corresponding to the usual HHG scenario when the wave packet of the recolliding electron is much broader than the characteristic size of the parent ion. Then, the electron's initial state for the recombination process is well approximated by a plane wave and the momentum is the only parameter that characterizes the electron. However, using specific setups one may control [31] and even focus the recolliding wave packet [32,33]. Let us discuss the optimization of recombination in the case when the dimension of the wave packet is comparable to or smaller than the characteristic size of the parent ion. Under these circumstances additional parameters arise, namely, the impact parameter of recollision and the size of the wave packet over which the recombination probability should be optimized.

Therefore, we proceed with the calculation of the recombination probability for a three-dimensional Gaussian wave packet which is localized in momentum space with a width Δ_p and an average momentum $\mathbf{p}$. In coordinate space the wave packet of the electron is focused at the parent ion. The wave packet passes the ionic core at the moment $t = 0$ with a width of the Gaussian wave packet Δ_s (see the scheme of the recollision in Fig. 4). It is then possible to define an impact parameter $\mathbf{b}$ perpendicular to its recolliding momentum p and give the wave function in momentum space:

$$\begin{aligned}\langle \mathbf{k}|\psi(t)\rangle = \frac{(4\ln 2)^{3/4}}{\pi^{3/4}\Delta_p^{3/2}} \times \exp\Bigg[&-2\ln 2\frac{(\mathbf{k}-\mathbf{p})^2 + i\gamma\mathbf{k}_\perp^2}{\Delta_p^2} \\ &-\frac{i\mathbf{k}^2 t}{2} + i\mathbf{k}\cdot\mathbf{b}\Bigg], \quad (14)\end{aligned}$$

where $\mathbf{k}_\perp$ is the momentum component perpendicular to $\mathbf{p}$. We have also included a possible chirp factor γ in the wave packet to vary the wave-packet size s in coordinate space perpendicular to the recolliding momentum p independently

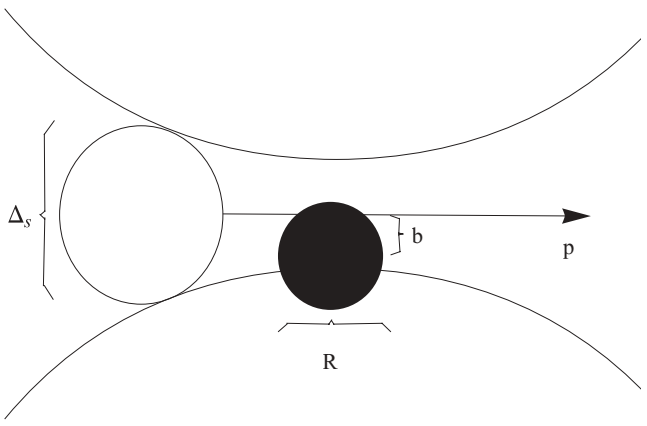

FIG. 4. Schematic picture of the recollision scenario. The black and the transparent circle represent the atomic system and the recolliding wave packet, respectively. The arrow gives the direction of the recolliding momentum p.

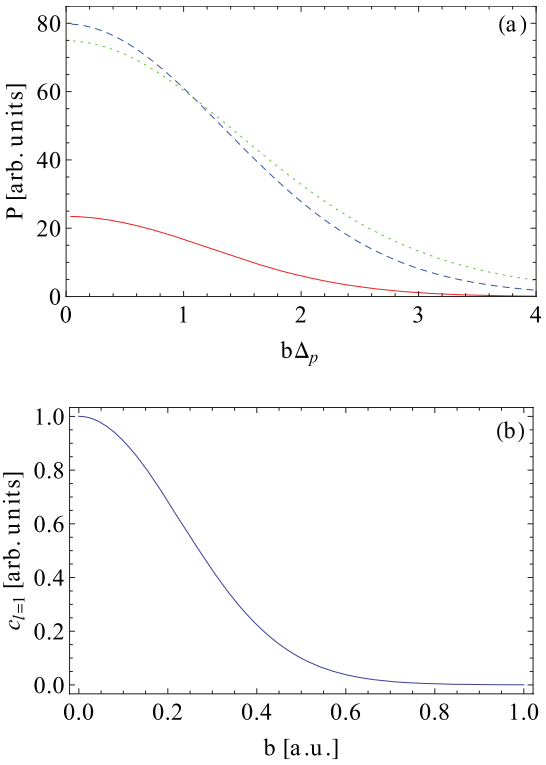

FIG. 5. (Color online) (a) Recombination probability versus $b\Delta_p$ for three different momentum space wave packet sizes: $\Delta_p = 2$ a.u. (red, solid), $\Delta_p = 5$ a.u. (blue, dashed), and $\Delta_p = 10$ a.u. (green, dotted) with $\kappa = 5$ a.u. and $p = 5$ a.u., and a chirping factor of $\gamma = 0$. (b) The amplitude of the p-wave component $c_{l=1}$ in the incoming electron wave packet of Eq. (14).

from Δ_p via $\Delta_s \approx 2.8\sqrt{1+\gamma^2}/\Delta_p$. The total recombination probability after the collision of the wave packet is given by

$$P = \int dt |\rho(t)|^2, \tag{15}$$

with

$$\rho(t) = \int d^3\mathbf{k} \langle \psi(t)|\mathbf{k}\rangle \langle \mathbf{k}|\tilde{\boldsymbol{\alpha}}_H \cdot \boldsymbol{\nabla} V(\mathbf{r})|\phi_0(t)\rangle, \tag{16}$$

with $\tilde{\boldsymbol{\alpha}}_H = \langle 0_H|\boldsymbol{\alpha}_H|1_H\rangle$. In Fig. 5 we plot the dependence of the recombination probability against the value of the impact parameter $|\mathbf{b}|$ for different sizes Δ_p of the wave packet in momentum space in a regime when the recolliding momentum is $p \sim \kappa$. We consider situations when the momentum width of the wave packet is smaller than the typical momentum of the atomic system ($\Delta_p \ll \kappa$) of the same size as the typical momentum of the atomic system ($\Delta_p \sim \kappa$) or larger than the typical momentum of the atomic system ($\Delta_p \gg \kappa$).

For all momentum widths the recollision is most likely when the impact parameter is zero. The recollision probability then decreases down to zero with increasing impact parameter b at a value that is comparable with the wave-packet size. This is because the recombination probability is determined by the p-wave component of the incoming electron wave packet:

$$\rho(t) = \int d^3\mathbf{k} \langle \psi(t)|\mathbf{k}\rangle \langle \mathbf{k}|k,(l=1)\rangle \times \langle k,(l=1)|\tilde{\boldsymbol{\alpha}}_H \cdot \boldsymbol{\nabla} V(\mathbf{r})|\phi_0(t)\rangle \tag{17}$$

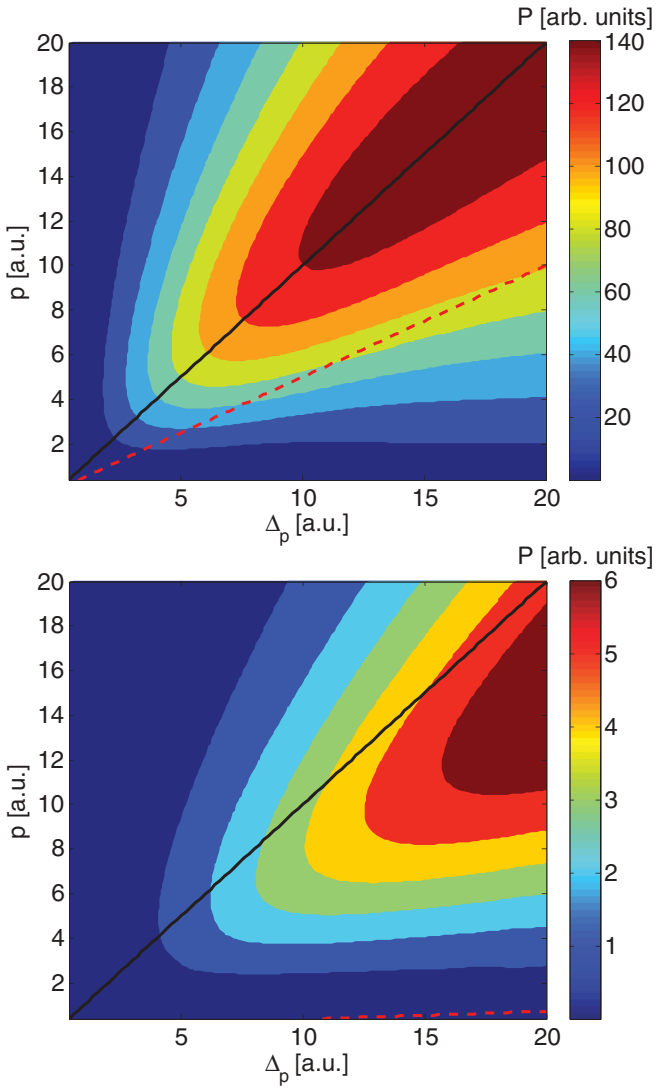

FIG. 6. (Color online) Recombination probability versus momentum width Δ_p and the recolliding momentum p for a central recollision with an atomic parameter of $\kappa = 5$ a.u.: (a) chirping factor $\gamma = 0$; (b) chirping factor $\gamma = 10$. The black line represents the relation $p/\Delta_p = 1$ and the dashed red line the relation $p\Delta_s = 1$.

with the p-wave state $|k,(l=1)\rangle$. However, the amplitude of the p-wave component $c_{l=1} = \int d^3\mathbf{k} \langle \psi(t)|\mathbf{k}\rangle \langle \mathbf{k}|k,(l=1)\rangle$ decreases with increasing impact parameter $\mathbf{b}$ [see Fig. 5(b)]. This is simply describing the situation when the electron misses the atomic core. Note that the recombination probability at the maxima of the curves in Fig. 5 depends on the value of the momentum width which is investigated in more detail below.

Further, we investigate the dependence of the recollision probability on the width of the wave packet in coordinate and momentum space. We choose the ideal case when the wave packet recollides centrally, i.e., $b = 0$. The width of the wave packet in coordinate and momentum space can be varied independently by means of the chirping factor γ. The recombination probability against the recolliding momentum p and the momentum width Δ_p are shown in Fig. 6 for two cases, either no chirp ($\gamma = 0$) or a large chirp ($\gamma = 10$). From Fig. 6 we can deduce a condition for optimal recombination:

approximately, the momentum width of the wave packet should be of the order of the recolliding momentum: $p \sim \Delta_p$. This is intuitively understandable as follows. At increasing the momentum spread of the wave packet Δ_p, the size of the wave packet decreases (focused electron beam) which increases the overlap of the incoming wave with the potential and, consequently, increases the recombination probability $\rho(t) = \langle\psi(t)|\tilde{\boldsymbol{\alpha}}_H \cdot \boldsymbol{\nabla} V(\mathbf{r})|\phi_0(t)\rangle$, while in the opposite limit $\Delta_p \gg p$, the damping behavior of the recombination matrix element Eq. (13) dominates. The large chirping factor of the wave packet, i.e., the increase of the size of the wave packet, generally decreases the recombination probability. However, the condition for the optimal recombination is still close to the rule $p \sim \Delta_p$ [see Fig. 6(b)]. As long as the optimal condition $p \sim \Delta_p$ is fulfilled, the chirp of the wave packet can be chosen arbitrarily in an experimental realization.

Thus, we come to the conclusion that for a very broad wave packet in momentum space the recombination with a high recolliding energy becomes feasible. We note that this conclusion is valid in the $\Delta_p > \kappa$ regime. In the opposite regime, when $\Delta_p < \kappa$, the wave packet can be considered as a plane wave and the discussion in Sec. III is applicable.

V. APPLICATIONS

In this section we apply the obtained optimal recollision rules to the HHG process. Let us consider HHG in a certain photon energy range, $\omega_H \sim 500$ eV, i.e., for a typical recollision momentum $p \sim E_0/\omega \sim \sqrt{2\omega_H} \approx 6$ a.u. Following Sec. III we will use hydrogenlike ions. Then, the mean separation of the ionic core and bound electron is given by $R = 1/\kappa$ and optimal recombination is expected when the recolliding momentum is of the order of the atomic potential parameter, i.e., $p \sim \kappa$. HHG in the given range can be realized using a suboptical laser, e.g., $\omega = 0.03$ a.u. and $E_0 = 0.4$ a.u. However, in this case the ionization potential $I_p = \kappa^2/2$ with $\kappa = 2$ a.u. is rather small, when the ionization rate is fixed via the parameter $E_0/\kappa^3 = 1/20$, where E_0 is the driving laser electric field strength. Consequently, the condition for optimal recollision will not be fulfilled. To fulfill the condition $p \sim \kappa$ at a given recollision energy due to fixed E_0/ω, the ionization potential should be larger such that $\kappa = 6$ a.u., i.e., $I_p \approx 490$ eV for hydrogenlike C^{5+}, which will require a stronger laser field $E_0 = 10.8$ a.u. ($I \approx 4 \times 10^{18}$ W/cm^2) and a larger laser frequency $\omega = 1$ a.u. $= 27.25$ eV from a FLASH laser [34]. In Fig. 7 two HHG spectra are calculated via Eq. (4), where the effect of the Coulomb force of the atomic core during ionization is taken into account via a correction factor [35] and the integral is evaluated via the saddle-point method [25]. They correspond to the case where the condition $p \sim \kappa$ is either fulfilled or where it is not when $p \gg \kappa$. We have fixed the recollision momentum via a cutoff energy at 3 keV and the ionization rate via the parameter $E_0/\kappa^3 = 1/20$. Then differences of the HHG emission rates in the two spectra can be traced back solely to the deviating spreading of the recolliding wave packet and the recombination probability. In the figure it is shown that the HHG emission probability for the parameters with $p \sim \kappa$ is about 6 orders of magnitude larger than for $p \gg \kappa$. This is mainly (4 orders of magnitude) due to the much larger recombination probability for the first parameter set. The

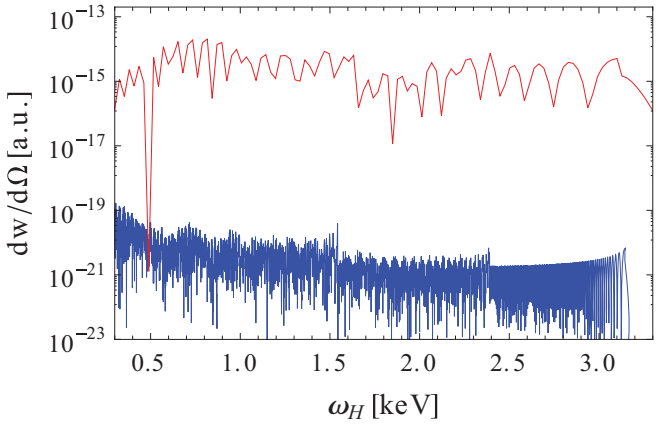

FIG. 7. (Color online) The HHG emission probability spectrum in laser polarization direction is displayed via Eq. (4) in two cases for a fixed ratio $E_0/\kappa^3 = 1/20$. In the upper curve (red) the parameters are the laser angular frequency $\omega = 1$ a.u. and the atomic parameter $\kappa = 6$ a.u., whereas in the lower curve we used $\omega = 0.03$ a.u. and $\kappa = 2$ a.u.. The employed step size in both curves is ω.

contribution of spreading is proportional to $E_0/(\kappa\omega^2)$ and is responsible for only 2 orders of magnitude. An estimation of the photon number per emitted pulse can be accomplished via Eqs. (8) and (9) of Ref. [36] for an emission window between 0.5 and 1 keV. Assuming a target gas density of $10^{17}/\text{cm}^3$ and a target gas diameter of 10 μm in the optimized scenario $p \sim \kappa$, a number of 10^4 photons per pulse is expected, whereas for the other case, when $p \gg \kappa$, less than one photon is emitted. This example shows that the judicious choice of the applied HHG parameters according to the optimal conditions can improve the efficiency of the HHG process significantly. For a fixed cutoff energy this suggests the use of high laser frequencies.

In a second scenario we show how the rule $p \sim \Delta_p$ discussed in Sec. IV can be taken advantage of to improve the HHG yield. We propose to employ such a strong laser field ($E_0 \sim \kappa^3/16$) that the ionization step takes place in the vicinity of the over-the-barrier mechanism. Then, the momentum distribution of the ionized wave packet will have the width of the bound-state momentum distribution that is of the order of κ. The latter is large enough to allow a fraction of the distribution to fulfill the condition for optimal recombination, i.e., $p \sim \kappa$ at the typical recollision momentum $p \sim E_0/\omega$ if the laser frequency is large enough. For example, with a feasible parameter set $\kappa = 6$ a.u., a laser electric field strength of $E_0 = 13.5$ a.u. ($I \approx 6.4 \times 10^{18}$ W/cm^2), and a laser angular frequency of $\omega \approx 2.2$ a.u. ≈ 61 eV this scenario can be realized.

VI. CONCLUSION

We have investigated the recombination step of HHG which represents the bottleneck in achieving HHG at high-photon energies and thus hinders the efficient hard x-ray generation via HHG. The influence of the atomic potential parameters as well as the parameters of the recolliding electron wave packet on the effectiveness of recollision are analyzed. The recombination takes place most efficiently for the recolliding electron momentum $p \lesssim \kappa$. In this regime the optimal condition is described by the so-called "$pR \sim 1$" rule, imposing a restriction on the characteristic size of the atomic

potential R. For the Coulomb potential in the $p \sim \kappa$ regime, the "$pR \sim 1$" rule is fulfilled automatically, indicating that hydrogenlike atoms and ions are already a good choice for the atomic system in the HHG process at $p \sim \kappa$. However, for large electron momenta this regime requires very large κ, i.e., high ionization potentials which are only available with highly charged ions. In the regime $p \gg \kappa$ and in the case of a broad recolliding electron wave packet $\Delta_p \ll p$, the recollision is optimal at $R \lesssim 1/p$; however, it decreases with rising momentum.

In the case of a focused electron wave packet $\Delta_p \gg \kappa$, the recombination is optimal when the momentum width of the wave packet is of the order of the recolliding momentum, the so-called $p \sim \Delta_p$ rule. This means that for a very broad wave packet in momentum space, the recombination with a high recolliding energy can be feasible.

APPENDIX

Here we show the exact continuum wave functions in the ZR, Coulomb, and box potential which have been used for the calculation of the recombination matrix element Eq. (5).

The wave function of the ground and continuum states in the ZR potential are [25,37]

$$\psi_0^Z(\mathbf{r}) = \sqrt{\frac{\kappa}{2\pi}}\frac{\exp[-\kappa r]}{r}, \quad \psi_{\mathbf{p}}^Z(\mathbf{r}) = \frac{1}{(2\pi)^{\frac{3}{2}}}\left(\exp[i\mathbf{p}\cdot\mathbf{r}] - \frac{\exp[ipr]}{(\kappa + ip)r}\right). \tag{A1}$$

The ground-state and continuum-state wave functions in Coulomb potential are

$$\psi_0^C(\mathbf{r}) = \sqrt{\frac{\kappa^3}{\pi}}\exp[-\kappa r], \quad \psi_{\mathbf{p}}^C(\mathbf{r}) = \frac{\Gamma\left[1+\frac{i\kappa}{p}\right]e^{-\frac{\pi\kappa}{2p}+i\mathbf{p}\cdot\mathbf{r}}\,{}_1F_1\left[-\frac{i\kappa}{p};1;ipr - i\mathbf{p}\cdot\mathbf{r}\right]}{2\sqrt{2}\pi^{3/2}}, \tag{A2}$$

and the ground-state and continuum-state wave functions in the box potential are

$$\psi_0^B(\mathbf{r}) = \begin{cases} \dfrac{\sin[r\sqrt{2V_0-\kappa^2}]}{\sqrt{2\pi}r\sqrt{\frac{1}{\kappa}+\frac{\pi}{\sqrt{2V_0-\kappa^2}}-\operatorname{arccot}\left(\frac{\kappa}{\sqrt{2V_0-\kappa^2}}\right)(2V_0-\kappa^2)^{-1/2}}}, & r < R \\ \dfrac{\exp[\kappa R-\kappa r]\sin[R\sqrt{2V_0-\kappa^2}]}{\sqrt{2\pi}r\sqrt{\frac{1}{\kappa}+\frac{\pi}{\sqrt{2V_0-\kappa^2}}-\operatorname{arccot}\left(\frac{\kappa}{\sqrt{2V_0-\kappa^2}}\right)(2V_0-\kappa^2)^{-1/2}}}, & r > R, \end{cases}$$

$$\psi_{\mathbf{p}}^B(\mathbf{r}) = \begin{cases} 2\sqrt{\frac{2}{3}}a_i\left(\frac{\sin(r\sqrt{p^2+2V_0})}{(p^2+2V_0)^{3/4}} - \frac{r\cos(r\sqrt{p^2+2V_0})}{\sqrt[4]{p^2+2V_0}}\right), & r < R \\ \frac{2i\sqrt{\frac{2}{\pi}}a_0 e^{ipr}(pr+i)}{p^{3/2}} - \frac{i\sqrt{\frac{2}{\pi}}(pr\cos[pr]-\sin[pr])}{p^2}, & r > R, \end{cases}$$

with

$$\begin{aligned} a_i = {} & \sqrt{\frac{3}{\pi}}pR(p^2+2V_0)^{3/4}(\sin[pR]+i\cos[pR])1/\{2p^2R\sqrt{p^2+2V_0}\cos[R\sqrt{p^2+2V_0}] \\ & -2i(p^3R+2pRV_0+2iV_0)\sin[R\sqrt{p^2+2V_0}]\} \end{aligned} \tag{A3}$$

and

$$\begin{aligned} a_0 = {} & \sqrt{\frac{3}{\pi}}e^{-ipR}\{\sin(R\sqrt{p^2+2V_0})[pR(p^2+2V_0)\cos[pR]-2V_0\sin(pR)] - p^2R\sqrt{p^2+2V_0}\sin(pR)\cos(R\sqrt{p^2+2V_0})\} \\ & \times 1/\{2\sqrt{p}[ip^2R\sqrt{p^2+2V_0}\cos(R\sqrt{p^2+2V_0}) + (p^3R+2pRV_0+2iV_0)\sin(R\sqrt{p^2+2V_0})]\}. \end{aligned} \tag{A4}$$

[1] P. Agostini and L. F. D. Mauro, Rep. Prog. Phys. **67**, 813 (2004).

[2] J. Seres, E. Seres, A. J. Verhoef, G. Tempea, C. Streli, P. Wobrauschek, V. Yakovlev, A. Scrinzi, C. Spielmann, and F. Krausz, Nature (London) **433**, 596 (2005).

[3] E. Seres, J. Seres, and C. Spielmann, Appl. Phys. Lett. **89**, 181919 (2006).

[4] T. Popmintchev, M.-C. Chen, A. Bahabad, M. Gerrity, P. Sidorenko, O. Cohen, I. P. Christov, M. Murnane, and H. C. Kapteyn, Proc. Natl. Acad. Sci. USA **106**, 10516 (2009).

[5] M.-C. Chen, P. Arpin, T. Popmintchev, M. Gerrity, B. Zhang, M. Seaberg, D. Popmintchev, M. M. Murnane, and H. C. Kapteyn, Phys. Rev. Lett. **105**, 173901 (2010).

[6] T. Popmintchev, M.-C. Chen, P. Arpin, M. M. Murnane, and H. C. Kapteyn, Nature Photon. **4**, 822 (2010).

[7] M. Kohler, T. Pfeifer, K. Z. Hatsagortsyan, and C. H. Keitel, arXiv:1201.5094v1 [Adv. At. Mol. Opt. Phys. (to be published)].

[8] A. Di Piazza, C. Müller, K. Z. Hatsagortsyan, and C. H. Keitel, arXiv:1111.3886v1 [Rev. Mod. Phys. (to be published)].

[9] M. C. Kohler, M. Klaiber, K. Z. Hatsagortsyan, and C. H. Keitel, Europhys. Lett. **94**, 14002 (2011).

[10] M. C. Kohler and K. Z. Hatsagortsyan, Phys. Rev. A **85**, 023819 (2012).

[11] K. J. Schafer, B. Yang, L. F. DiMauro, and K. C. Kulander, Phys. Rev. Lett. **70**, 1599 (1993).

[12] P. B. Corkum, Phys. Rev. Lett. **71**, 1994 (1993).
[13] M. Lewenstein, P. Balcou, M. Y. Ivanov, A. L'Huillier, and P. B. Corkum, Phys. Rev. A **49**, 2117 (1994).
[14] M. Y. Ivanov, T. Brabec, and N. Burnett, Phys. Rev. A **54**, 742 (1996).
[15] A. M. Perelomov, V. S. Popov, and V. M. Terent'ev, Zh. Eksp. Teor. Fiz. **52**, 514 (1967).
[16] M. V. Ammosov, N. B. Delone, and V. P. Krainov, Zh. Eksp. Teor. Fiz. **91**, 2008 (1986).
[17] Z. Chen, A.-T. Le, T. Morishita, and C. D. Lin, Phys. Rev. A **79**, 033409 (2009).
[18] A. Gordon, F. X. Kärtner, N. Rohringer, and R. Santra, Phys. Rev. Lett. **96**, 223902 (2006).
[19] M. Y. Amusia, N. B. Avdonina, L. V. Chernysheva, and M. Y. Kuchiev, J. Phys. B **18**, L791 (1985).
[20] A. V. Korol, F. J. Currell, and G. F. Gribakin, J. Phys. B **37**, 2411 (2004).
[21] A. D. Shiner, B. E. Schmidt, C. Trallero-Herrero, H. J. Wörner, S. Patchkovskii, P. B. Corkum, J-C. Kieffer, F. Légaré, and D. M. Villeneuve, Nat. Phys. **7**, 464 (2011).
[22] L. V. Keldysh, Zh. Eksp. Teor. Fiz. **47**, 1945 (1964).
[23] F. H. M. Faisal, J. Phys. B **6**, L89 (1973).
[24] H. R. Reiss, Phys. Rev. A **22**, 1786 (1980).
[25] D. B. Milošević and W. Becker, Phys. Rev. A **66**, 063417 (2002).
[26] W. Becker, F. Grasbon, R. Kopold, D. Milošević, G. G. Paulus, and H. Walther, Adv. At., Mol., Opt. Phys. **48**, 36 (2000).
[27] A. Gordon and F. X. Kärtner, Phys. Rev. Lett. **95**, 223901 (2005).
[28] G. Jordan and A. Scrinzi, New J. Phys. **10**, 025035 (2008).
[29] L. D. Landau and E. M. Lifshitz, *Quantum Mechanics* (Pergamon, Oxford, 1977).
[30] H. A. Bethe and E. E. Salpeter, *Quantum Mechanics of One- and Two-Electron Atoms* (Academic Press, New York, 1957).
[31] C. Liu, M. Kohler, K. Z. Hatsagortsyan, and C. H. Keitel, New J. Phys. **11**, 105045 (2009).
[32] N. Milosevic, P. B. Corkum, and T. Brabec, Phys. Rev. Lett. **92**, 013002 (2004).
[33] M. Verschl and C. H. Keitel, Phys. Rev. ST Accel. Beams **10**, 024001 (2007).
[34] The Free-Electron Laser in Hamburg (FLASH) (2011), [http://hasylab.desy.de/facilities/flash/index_eng.html].
[35] V. Krainov, J. Opt. Soc. Am. B **14**, 425 (1997).
[36] J. C. Liu, M. C. Kohler, C. H. Keitel, and K. Z. Hatsagortsyan, Phys. Rev. A **84**, 063817 (2011).
[37] W. Becker, J. K. McIver, and M. Confer, Phys. Rev. A **40**, 6904 (1989).
[38] $P \sim |\alpha_H p V_p|^2 \sim |V_p|^2/p^4$, because $\alpha_H \sim 1/\omega_H^{3/2} \sim 1/p^3$ in the limit $p \gg \kappa$. The harmonic photon energy ω_H is determined by the recolliding electron energy.